Journal of Electroceramics, 14, 37–44, 2005

Epitaxial Pb(Zr,Ti)O_3 Capacitors on Si by Liquid Delivery Metalorganic Chemical Vapor Deposition

S.Y. YANG,[1,*] B.T. LIU,[1] J. OUYANG,[1] V. NAGARAJAN,[1] V.N. KULKARNI,[1] R. RAMESH,[1] J. KIDDER,[2] R. DROOPAD[3] & K. EISENBEISER[3]

[1]*Department of Materials Science and Engineering, Center for Superconductivity Research, University of Maryland, College Park, MD 20742*

[2]*Department of Mechanical Engineering, Vermont Technical College, Randolph Center, VT 05061*

[3]*Physical Science Research Laboratories, Motorola Laboratories, Tempe, Arizona 85284*

Submitted September 3, 2003; Revised March 11, 2004; Accepted March 16, 2004

Abstract. $La_{0.5}Sr_{0.5}CoO_3/Pb(Zr_xTi_{1-x})O_3/La_{0.5}Sr_{0.5}CoO_3$ capacitors have been successfully fabricated by liquid delivery metalorganic chemical vapor deposition on Si wafers using $SrTiO_3$ thin layer (20 nm) as a template. $Zr(dmhd)_4$ in tetrahydrofuran was used as Zr precursor for compatible thermal behavior with $Pb(thd)_2$ and $Ti(OiPr)_2(thd)_2$ precursors. The dependence of the ferroelectric film composition on the precursor mixing ratio and growth temperature has been systematically studied by Rutherford Backscattering (RBS). Ferroelectric and piezoelectric properties at the composition close to morphotropic phase boundary region ($Pb(Zr_{0.5}Ti_{0.5})O_3$) have been investigated for application in nonvolatile ferroelectric random access memories and microelectromechanical system (MEMS). These capacitors show desirable ferroelectric properties, which proves that this approach is very promising for both fundamental study and potential applications. The changes of spontaneous polarization (P_s) and piezoelectric coefficient (d_{33}) with Ti/(Zr + Ti) ratio are also presented and compared with theoretical values.

Keywords: PZT, liquid delivery MOCVD, $Zr(dmhd)_4$, $SrTiO_3$ template layer, LSCO/PZT/LSCO capacitors

1. Introduction

Lead zirconate titanate (PZT) ferroelectric thin films have been extensively studied as candidates for use in nonvolatile ferroelectric random memories (FeRAMs) [1–3], field effect devices [4, 5], microelectromechanical systems (MEMS) [6], and pyroelectric sensors [7]. Efforts to integrate ferroelectric thin films with Si-CMOS technology have been greatly increased to enable commercially viable, high-density, nonvolatile ferroelectric memories and other devices. Up to date, there has been significant progress in the growth of epitaxial oxides on semiconductors [8–11]. Of specific interest is the development of epitaxial $SrTiO_3$ (STO) on silicon for use as an alternative gate dielectric [12–14]. By using insulating STO layer as a template/barrier, we have recently succeeded in seeding the epitaxial growth of ferroelectric layers by a Sol-Gel method [15].

The STO layer allows the growth of a highly textured/epitaxial film, ensuring high polarization as well as uniform properties over large scales and small feature sizes. Such an approach is especially important when the ferroelectric grain size is commensurate with that of the lateral dimensions of the storage cell. Presently, various film synthesis techniques, such as Pulsed Laser Deposition (PLD) [16, 17], Sol-Gel [18, 19], Sputtering [20], and Metalorganic Chemical Vapor Deposition (MOCVD) [21–23], have been employed to prepare PZT films. Among these deposition techniques, MOCVD offers the greatest potential advantages because of its good conformal step coverage, controllability of composition, high deposition rate and compatibility with current Si processes. MOCVD of PZT films was first adopted in the early 1990s and significant progress has been made to optimize the

*To whom all correspondence should be addressed. E-mail: svyang@wam.umd.edu

process control of growth parameters, precursor delivery method, and precursor chemistry. A considerable number of advances have occurred in the area of precursor development as well as delivery techniques. For example, although bis(tetramethylheptanedionate)lead, $Pb(thd)_2$, a nontoxic and safer precursor compared to alkyl Pb sources, has been recently used as a Pb source, it has a low vapor pressure and needs high temperature to produce sufficient gas phase supply. This is a disadvantage, because the precursor properties are degraded over time. In order to avoid this, we have used a liquid delivery system, which can reduce the thermal budget and prevent degradation of precursors. In this case, however, all the precursors must have similar thermal properties such as vaporization and decomposition temperature because the mixture is vaporized (as opposed to vaporizing individual precursors) and decomposed at growth temperature. The Zr precursor usually needs higher temperature for vaporization compared with Ti and Pb precursors; therefore, selecting a Zr precursor with low vaporization temperature is critical for consistent vaporizer behavior. Tetrakis(dimethylheptanedionate)-zirconium, $Zr(dmhd)_4$ in tetrahydrofuran (THF) was used as Zr precursor in our experiments instead of commonly used $Zr(thd)_4$ because its vaporization temperature is about 25–30°C lower than that of $Zr(thd)_4$. The good thermal compatibility of $Zr(dmhd)_4$ with $Pb(thd)_2$ and di(isopropoxyde)bis-(tetramethylheptanedionate)titanium, $Ti(OiPr)_2(thd)_2$ was confirmed by thermogravimetric (TG) curves measured at 1 atm Ar atmosphere as shown in Fig. 1. By

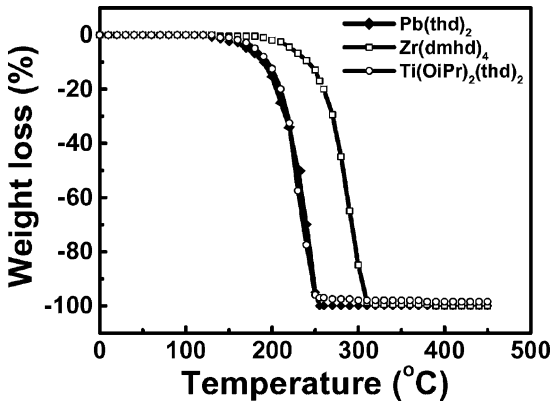

Fig. 1. The thermogravimetric (TG) curves show the good thermal compatible behavior for $Zr(dmhd)_4$ with $Pb(thd)_2$ and $Ti(OiPr)_2(thd)_2$.

using $Zr(dmhd)_4$, $Pb(thd)_2$ and $Ti(OiPr)_2(thd)_2$ in THF as precursors in our experiments, we have successfully deposited PZT films on Si using STO as a template. In this article, we report the structural and physical properties of $LaSrCoO_3/Pb(Zr_xTi_{1-x})O_3/LaSrCoO_3$ (LSCO/PZT/LSCO) capacitors, which can provide a solution to the polarization fatigue problem. In addition, dependence of PZT film composition with the precursor mixing ratio, growth temperature, and switching properties of epitaxial $Pb(Zr_{0.5}Ti_{0.5})O_3$ capacitors are addressed.

2. Experiments

70 nm of LSCO electrode, which enables fatigue-free PZT capacitors, was deposited at room temperature on STO/Si by RF sputtering with a power of 300 W for 30 min using an $Ar:O_2$ (5:1) mixture. The samples were then annealed at 600–650°C in an oxygen-flowing tube furnace to obtain an epitaxial LSCO buffer layer for seeding epitaxial PZT films. PZT films were prepared by liquid delivery metalorganic chemical vapor deposition (MOCVD). The schematic of the MOCVD system is shown in Fig. 2. In our experiments, 0.3 mol/L $Pb(thd)_2$ in THF, 0.3 mol/L $Ti(OiPr)_2(thd)_2$ in THF and 0.3 mol/L $Zr(dmhd)_4$ in THF (all from Mitsubishi Materials Corporation) were used as precursors.

Three liquid precursors were mixed at specified volumetric ratios in a computer controlled mixing manifold and then transported to the vaporization cell. Vaporized source gas was transported by high-purified Ar carrier gas to a vertical type chamber. All the downstream parts, including the chamber, were heated to a temperature of 10°C higher than the vaporizer temperature to avoid condensation of gas phase source material. The chamber was pumped to a base pressure of 1×10^{-3} Torr prior to ramping the temperature of the substrate heater. High-purity O_2 was used as an oxidizing gas during the deposition that was performed at various substrate temperatures, ranging from 450 to 650°C. The deposition rate was in excess of 130–150 A/min at 650°C. The detailed deposition parameters are summarized in Table 1. To complete the capacitor stack, Pt/LSCO was deposited as the top electrode on 32–50 μm diameter circular pads defined using standard lithography processes. X-ray diffraction (XRD) and transmission electron microscopy (TEM) have been used to study the structure of the PZT films. Rutherford Backscattering (RBS) was employed to study the composition of PZT with various deposition conditions.

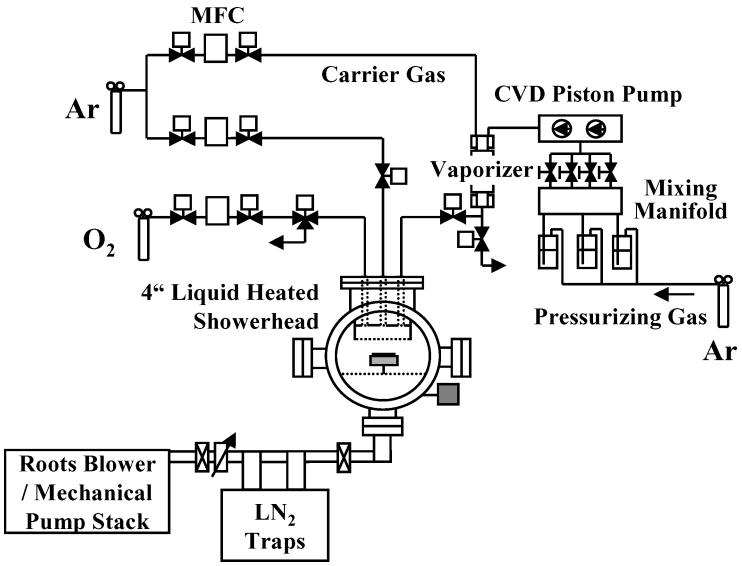

Fig. 2. The schematic of liquid delivery MOCVD system.

A 2.00 MeV $4He^+$ ion beam was directed at normal incidence to the sample surface and then detected at a scattering angle of 168°. The ferroelectric properties were characterized using a RT6000 tester (Radiant Technologies) and the out-of-plane piezoelectric response (d_{33}) was measured using a scanning piezo force microscope [24].

3. Results and Discussion

3.1. Control of Deposition Parameters and Growth Characteristics

In order to fully control the MOCVD deposition process, we have tried to map the ratio of Zr/(Zr + Ti) in $Pb(Zr_xTi_{1-x})O_3$ films as a function of the Zr and Ti precursor ratios (V(Zr)/V(Ti)). In this study x ranged from 0.2 to 0.8 at a deposition temperature of 650°C. We also investigated the dependence of PZT composition with various temperatures at specific precursor ratios. Figure 3(a) shows the relationship of RBS measured Zr/(Zr + Ti) atomic ratio in the PZT films versus precursor source mixing ratios. The volumetric ratio of Pb was fixed between 20–30% to get a proper stoichiometric composition of Pb/(Pb + Zr + Ti).

Table 1. Deposition parameters of PZT films prepared by liquid delivery MOCVD.

Substrate	LSCO/$SrTiO_3$/Si
Precursors	$Pb(thd)_2$
	$Zr(dmhd)_4$
	$Ti(OiPr)_2(thd)_2$
Vaporizer temperature	210°C
Carrier gas (Ar) flow rate	200 sccm
O_2 gas flow rate	500 sccm
Substrate temperature	450–650°C
Process pressure	2 Torr
Liquid solution flow rate	0.2 ml/min

Even though the entire range of compositions ($0 < Zr/(Zr + Ti) < 1$) of PZT films could be obtained with proper solution mixing ratios, non-ideal solution behavior was observed. Keijser et al. experimentally determined a non-ideality factor for a conventional bubbler system where each precursor was thermally controlled separately [22]. Non-ideality factor (K) can be obtained by the following equation,

$$\frac{x}{1-x} = K\frac{x_g}{1-x_g} \tag{1}$$

where, x and x_g denote Zr/(Zr + Ti) ratio in film and gas phase, respectively. As an approximation, we assume x_g can be directly replaced with x_l (liquid mixing ratio of Zr/(Zr + Ti)). The obtained K value was 2.6, which is higher than the result of 1.49 reported by Keijser et al. While conventional bubbler systems deliver each precursor seperately, liquid delivery systems,

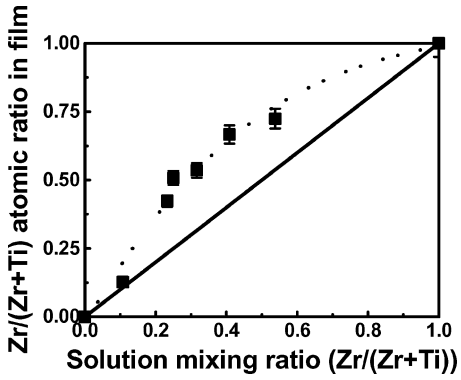

(a)

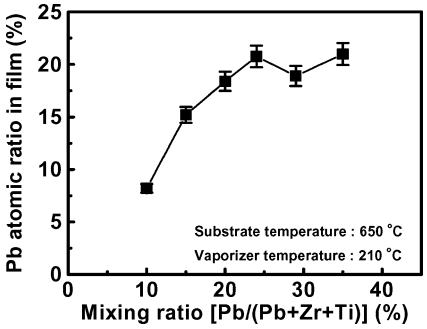

(b)

Fig. 3. (a) The relation of atomic percent of Pb, Zr and Ti of PZT films was measured by RBS with precursor mixing ratio prepared at 650°C and the same volume ratio (V(Pb)/V(Zr) = 1) of Pb and Zr precursors was used during deposition at 650°C. (b) The variation of Pb atomic percent grown at 650°C with different supply flow rate.

have only one hot vaporization cell where mixtures of three different precursors are vaporized simultaneously and then delivered to the chamber together. Since the three precursors have different thermal properties, such as evaporation temperature and thermal volatility, volumetric solution mixing ratio can not be same as the supply gas ratio of each component at a fixed temperature which means that x_l is not equivalent to x_g and other calibration factors must be added to Eq. (1) to compensate for different thermal volatility. Even though the K's for liquid and gas delivery are not physically equivalent, they are still useful in describing the relative ease of composition control, independent of delivery method. Despite the relatively high non-ideality factor, we were still able to reproducibly control film composition. Figure 3(b) shows the variation of Pb concentration in the film with changing supply mixing ratio at a substrate temperature of 650°C. Pb concentration in the film became saturated at a supply mixing ratio of 20%. This behavior is consistent with the well-known Pb concentration self-regulation mechanism. This self-regulation behavior can be explained by the existence of an equilibrium state between adsorption to substrate surface and desorption to gas phase. The higher vapor pressure of PbO compared with ZrO_2 and TiO_2 allows it to be readily re-evaporated from substrate at high temperature. Competitive reactions between adsorption and re-evaporation on the substrate results in a plateau, which can be used as process window.

3.2. *Structural and Electrical Properties of $Pb(Zr_{0.5}Ti_{0.5})$ Films*

A solution mixing ratio of 20:20:60 with Pb:Zr:Ti enables us to get $Pb(Zr_{0.5}Ti_{0.5})O_3$ films. This composition is close to the morphotropic phase boundary (MPB), which possesses a lower coercive field, and large d_{33}.

A typical θ–2θ X-ray diffraction scan of LSCO/PZT/LSCO is shown in Fig. 4, indicating that the LSCO/PZT/LSCO heterostructure is highly [*00l*] oriented without any secondary phase. The in-plane ϕ-scan around the (101) peak shown in the inset in Fig. 4 further confirms that the films grow with the expected four-fold symmetry. A c-axis lattice parameter of 4.08 Å was calculated from the diffraction patterns.

The capacitors were subjected to a variety of stringent electrical tests to probe their performance characteristics. The hysteresis loops of 230 nm thick PZT films measured at 1, 3, and 5 V are shown in Fig. 5(a). The measured resistivity was found to be on the order

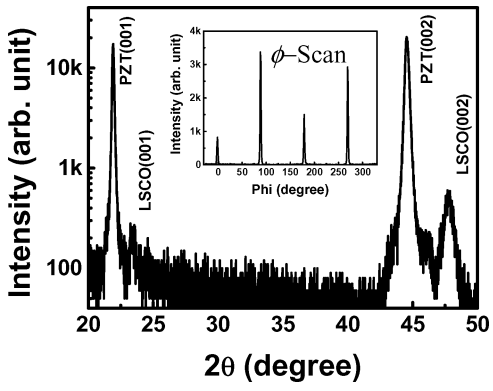

Fig. 4. A typical θ-2θ X-ray diffraction scan and ϕ-scan of LSCO/PZT/LSCO capacitors deposited on STO/Si at 650°C.

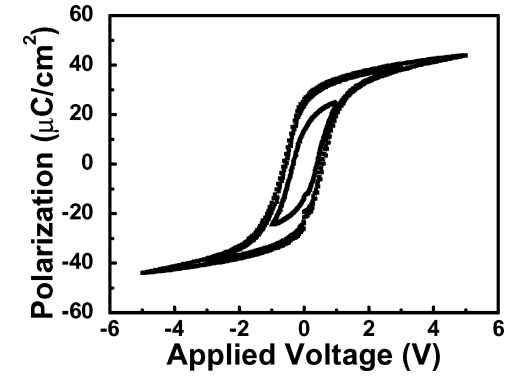

(a)

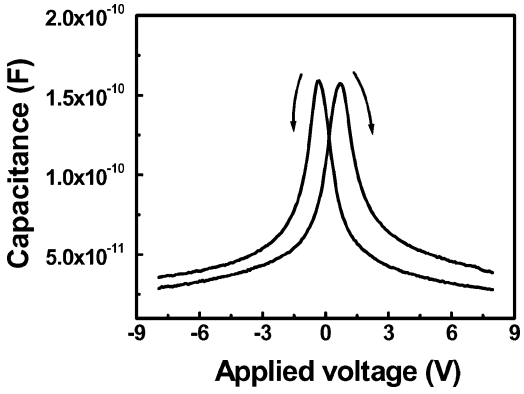

(b)

Fig. 5. (a) The hysteresis response of 230 nm thick $Pb(Zr_{0.5}Ti_{0.5})$ capacitor sandwiched by LSCO electrodes at 1, 3 and 5 V. (b) Capacitance vs applied voltage measured with 230 nm thick $Pb(Zr_{0.5}Ti_{0.5})$ capacitor sandwiched by LSCO electrodes.

of 4–8 $\times$ 10^{10} Ω-cm. The remanent polarization (P_r) and coercive field (E_c) measured at 3 V were about 25 μC/cm^2 and 27.5 kV/cm, and about 31 μC/cm^2 and 30 kV/cm at 5 V, respectively. This high polarization and low coercive field are very favorable for FeRAMs application. Capacitance curves measured on this film are shown in Fig. 5(b). The measurements were made for disk shape capacitors with an area of 2.2×10^{-5} cm^2. We measured a capacitance of 158 pF at 6390 Hz, and the dielectric constant (ε_r) calculated from this value is 1600 at peak points. This value is close to the results obtained for films of similar compositions and thicknesses grown by CVD [23]. In order to further characterize the capacitors, the pulsed polarization ($\Delta P = P^* - P$) as a function of applied voltage is displayed in Fig. 6. It indicates a pulsed polarization value of 34 and 36 μC/cm^2 corresponding to 3 and 5 V,

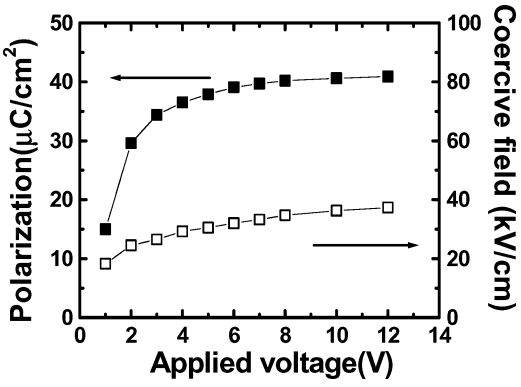

Fig. 6. Polarization (switched (P^*) – non-switched ($P\hat{}$)) and coercive voltage of LSCO/PZT/LSCO capacitors as a function of applied voltage.

respectively. In addition, the coercive field versus the applied voltage is shown in the same figure. This figure shows that it saturates with increasing the applied voltage; the coercive field is only 37.3 kV/cm (0.75 V) at 12 V, which is consistent with the properties of PZT near MPB [25] and ideal for low voltage application.

Figure 7 shows the dependence of pulsed polarization (ΔP) on pulse-width. A key point of reference is the value of this pulse polarization at a pulse width of 1 μsec. The LSCO/PZT/LSCO capacitors show favorable pulse width dependence, i.e. the polarization measured at 5 V is 33 μC/cm at 1 μsec pulse width and increases to about 40 μC/cm^2 at 1000 μsec. It is still 23 μC/cm^2 at 3 V for a pulse width of 1 μsec. Quantitative fits of the pulse width dependence for the samples yield a slope that is essentially constant (2.5–3 μC/cm^2

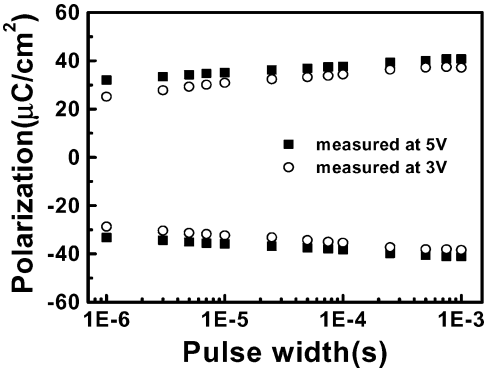

Fig. 7. Pulse-width dependence of polarization (switched (P^*) – non-switched ($P\hat{}$)) of LSCO/PZT/LSCO capacitors measured at 3 and 5 V, respectively.

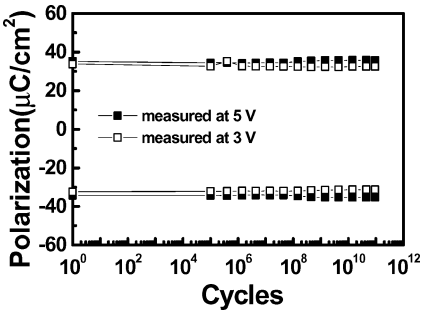

Fig. 8. Fatigue resistant characteristics of LSCO/PZT/LSCO capacitors as a function of bipolar-pulsed cycles measured at 3 and 5 V, respectively.

per decade) although the slope measured at 5 V is slightly smaller. The weak pulse-width dependence of polarization for the samples prepared by MOCVD demonstrates that these capacitors are promising candidates for high-speed FeRAM application.

Our previous results have clearly demonstrated that the use of a conducting perovskite electrode (such as LSCO) can eliminate polarization fatigue [26]. Figure 8 shows the test capacitors subjected to polarization fatigue testing via bipolar-pulsed cycles of both 3 and 5 V at 1 MHz. Fatigue characteristics of LSCO/PZT/LSCO capacitors measured at different voltages shows no observable degradation up to 10^{11} cycles.

The piezoelectric hysteresis loops for this MPB composition samples were measured by using piezoresponse microscopy, which has been successfully used to characterize piezoelectric properties of PZT capacitors [27, 28]. Figure 9 shows the piezoelectric hysteresis loops obtained from 230 nm- and 3 μm-thick

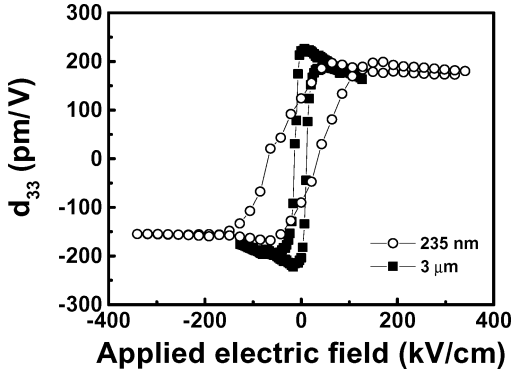

Fig. 9. Piezoelectric hysteresis loops of 230 nm and 3 μm-thick $Pb(Zr_{0.5}Ti_{0.5})$ films. (-○- 230 nm $Pb(Zr_{0.5}Ti_{0.5})$ films; -■- 3 μm-thick $Pb(Zr_{0.5}Ti_{0.5})$ films.)

$Pty(Zr_{0.5}Ti_{0.5})$ films. The obtained maximum longitudinal piezoelectric coefficients, i.e., d_{33}, were 199 and 208 pm/V, respectively, which are higher than values reported by other studies but still smaller than bulk value. Further analysis on d_{33} values of films compared to that of bulk will be discussed in Section 3.3.

3.3. Comparison of Piezoelectric Properties of Different Thickness and Composition

As indicated in previous section, the PZT family of ceramics is widely used in piezoelectric and dielectric applications. It was reported that compositions near the morphotropic phase boundary (MPB) have the largest piezoelectric constants [29]. Especially, [001] oriented bulk PZT shows maximum values of 327 pm/V for the tetragonal phase and above 500 pm/V for the rhombohedral phase as shown in Fig. 11. In our study, PZT films with different thickness from 230 nm to 5 μm were fabricated and piezoelectric properties were measured and compared with bulk values.

In order to avoid the complication induced by large discontinuity of d_{33} between tetragonal and rhombohedral structures, we identified the structure of all the samples. Careful measurements were performed by ϕ-scan and in plane lattice parameter measurement. All the samples showed four-fold symmetry, which reveals the cube-on-cube epitaxy, and tetragonal structure was confirmed by calculation of c/a ratio (between 1.005 and 1.01). The obtained c/a values, which are smaller than that of bulk (1.025), illustrates the in-plane tensile stress in PZT films induced by the thermal mismatch between films and the Si substrate.

Figure 10 showed the variation of d_{33} values and coercive fields obtained from 230 nm, 1 μm, 3 μm and 5 μm thick films. The obtained d_{33} values showed almost constant values between 199 and 225 pm/V within experimental error, while coercive field decreased sharply up to 1 μm and saturated at 10 kV/cm. In our previous study, we demonstrated the effect of misfit on d_{33}, where the d_{33} of PZT films on Si substrate were theoretically predicted. The obtained values in this study agree well with our previous results [24].

We have further investigated the compositional dependence of d_{33} on the $Zr/(Zr + Ti)$ ratio. All the samples were prepared with the thickness at 230 ± 20 nm. Figure 11 demonstrates the relationship of experiment measured film d_{33} and the theoretical bulk d_{33} (by Haun et al.) with the composition of PZT films [30].

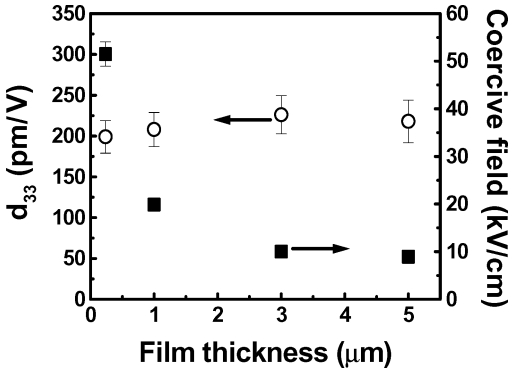

Fig. 10. The changes of piezoelectric coefficient (d_{33}) and coercive field (E_c) with film thickness. (♀ d_{33} of PZT films; ■ E_c of PZT films.)

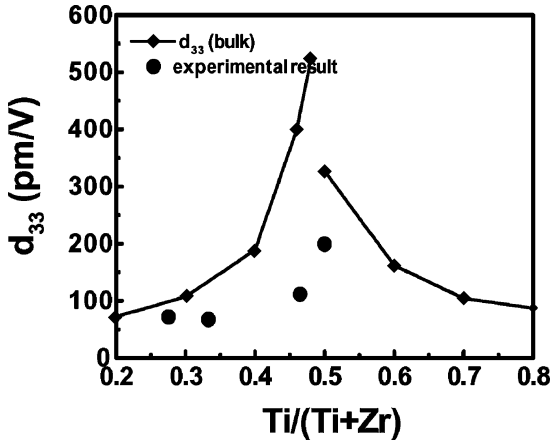

Fig. 11. The changes of piezoelectric coefficient (d_{33}) with change of Ti/(Zr + Ti) ratio. (-♦- d_{33} of bulk PZT calculated by Haun et al.; ● d_{33} of thin PZT obtained from experiment at the present study.)

The maximum d_{33}, 199 pm/V, was obtained at MPB composition. This tendency is in good agreement with those of bulk PZT. However, it should be mentioned that it is still smaller than theoretical value. This may be caused by several factors, for example, the clamping from substrate [24], which can be reduced by creating sub-micron islands of PZT capacitors (by Focused Ion Beam etching (FIB)). Accordingly, we have obtained d_{33} values close to theoretical prediction from FIB processed PZT capacitors where PZT films were prepared by pulsed laser deposition (PLD) [24]. These results suggest that d_{33} values are substantially suppressed in continuous films by the clamping from the substrate, whereas it can be improved by creating sub-micron PZT capacitors.

4. Conclusion

In summary, we have demonstrated an epitaxial perovskite template approach that has enabled us to create LSCO/ PZT/LSCO ferroelectric capacitors prepared by MOCVD on silicon substrates. The relationship of PZT film composition with the precursor mixing ratio and growth temperature has been systematically studied so that a PZT film of specific composition can be easily prepared. Ferroelectric properties of 230 nm thick $Pb(Zr_{0.5}Ti_{0.5})O_3$ capacitors, close to MPB, have been specifically reported as an example. The remanent polarization and coercive voltage measured at 3 V are about 25 $\mu C/cm^2$ and 0.55 V, and at 5 V about 31 $\mu C/cm^2$ and 0.6 V, respectively. No obvious degradation of polarization can be observed up to 10^{11} switching cycles. Also high resistivity and small pulse width dependence characteristics as described above show the approach of epitaxial capacitors fabricated on Si wafers robust. The piezoelectric coefficients, d_{33} values, of PZT films reached 210 ± 10 pm/v for the thickness range from 230 nm to 5 μm.

Acknowledgment

This work is supported by the NSF-MRSEC under Contract No. DMR-00-80008.

References

1. O. Auciello, J.F. Scott, and R. Ramesh, *Physics Today*, **22** (1998).
2. S. Aggarwal, A.M. Dhote, H. Li, S. Ankem, and R. Ramesh, *Appl. Phys. Lett.*, **74**, 230 (1999).
3. H.N. Al-Sharreef, B.A. Turtle, W.L. Warren, D. Dimos, and M.V. Raymond, *Appl. Phys. Lett.*, **68**, 272 (1996).
4. B.T. Liu, Z. Hao, Y.F. Chen, B. Xu, H. Chen, F. Wu, and B.R. Zhao, Yu. Kislinskii, and E. Stepantsov, *Appl. Phys. Lett.*, **74**, 2044 (1999).
5. T. Wu, S.B. Ogale, J.E. Garrison, B. Nagaraj, Amlan Biswas, Z. Chen, R.L. Greene, R. Ramesh, and T. Venkatesan, *Phys. Rev. Lett.*, **86**, 5998 (2001).
6. Ing-Shin Chen, Jeffrey F. Roeder, Dong-Joo Kim, Jon-Paul Maria, and Angus I. Kingon, *J. Vac. Sci. Technol. B*, **19**, 1833 (2001).
7. S.A. Impey, Z. Huang, A. Patel, R. Beanland, N.M. Shorrocks, R. Watton, R. Watton, and R.W. Whatmore, *J. Appl. Phys.*, **83**, 2202 (1998).
8. T. Yamaguti, *Proc. Phys. Math. Soc. Jpn.*, **17**, 443 (1935).
9. R. Sato, *J. Phys. Soc. Jpn.*, **6**, 527 (1951).
10. M. Diara, Y. Arimoto, M. Jifuku, T. Kimura, S. Kodama, H. Yamawaki, and T. Yamaoka, *J. Electrochem. Soc.*, **129**, 2569 (1982).

11. U.S. Matsubara, N. Shohata, and M. Mikami, *Jpn. J. Appl. Phys., Suppl.*, **24**, 10 (1985).
12. R.A. McKee, F.J. Walker, and M.F. Chisholm, *Phys. Rev. Lett.*, **81**, 3014 (1998).
13. A. Lin, X. Hong, V. Wood, A.A. Verevkin, C.H. Ahn, R.A. Mckee, F. Walker, and E.D. Specht, *Appl. Phys. Lett.*, **78**, 2034 (2001).
14. K. Eisenbeiser, J.M. Finder, Z. Yu, J. Ramdani, J.A. Curless, J.A. Hall-mark, R. Droopad, W.J. Ooms, L. Salem, S. Bradshaw, and C.D. Over-gaard, *Appl. Phys. Lett.*, **76**, 1324 (2000).
15. Y. Wang, C. Ganpule, B.T. Liu, H. Li, K. Mori, B. Hill, M. Wuttig, R. Ramesh, J. Finder, Z. Yu, R. Droopad, and K. Eisenbeiser, *Appl. Phys. Lett.*, **80**, 97 (2000).
16. J.S. Hrowitz, K.S. Grabowski, K.B. Chrisey, and R.E. Leuchtner, *Appl. Phys. Lett.*, **59**, 1565 (1991).
17. R. Ramesh, T. Sands, and V.G. Keramidas, *J. Electron. Mater.*, **23**, 19 (1994).
18. H.N. Al-Shareff, K. Bellur, O. Auciello, and A.I. Kingon, *Ferroelectrics*, 152, **85** (1994).
19. Y. Shimizu, K.R. Udayakumar, and L.E. Cross, *J. Am. Ceram. Soc.*, **74**, 3023 (1991).
20. T. Fukami, I. Mimenmura, Y. Hiroshima, and T. Osada, *Jpn. J. Appl. Phys.*, **130**, 2155(1991).
21. C.M. Foster, R. Csencsits, G.R. Bai, Z. Li, L.A. Wills, R. Hiskes, H.N. Al-Shareef, and D. Dimos, *Int. Ferroelectric*, **10**, 3 (1995).
22. M. De Keijser, P.J. Van Veldhoven, and G.J.M. Dormans, *Mat. Res. Soc. Symp. Proc.*, **310**, 223 (1993).
23. P.K. Larsen, G.J.M. Dormans, D.J. Taylor, and P.J. Van Veldhoven, *J. Appl. Phys.*, **76**, 2405 (1994).
24. V. Nagarajan, A. Stanishevsky, L. Chen, T. Zhao, B.T. Liu, J. Mehlgailis, A.L. Roytburd, and R. Ramesh, *Appl. Phys. Lett.*, **81**, 4215 (2002).
25. A.H. Carim, B.A. Turtle, D.H. Doughty, and S.L. Martinez, *J. Am. Ceram. Soc.*, **74**, 1455 (1991).
26. R. Ramesh, W.K. Chan, B. Wilkens, H. Gilchrist, T. Sands, J.M. Tarascon, V.G. Keramidas, D.K. Fork, J. Lee, and A. Safari, *Appl. Phys. Lett.*, **61**, 1537 (1992).
27. P. Muralt, *J. Micromech. Microeng.*, **10**, 136 (2000).
28. C.S. Ganpule, A. Stanishevsky, Q. Su, S. Aggarwal, J. Mengailis, E. Williams, and R. Ramesh, *Appl. Phys. Lett.*, **75**, 4091 (1999).
29. Dennis L. Polla and Lorraine F. Francis, *Annu. Rev. Mater. Sci.*, **28**, 563 (1998).
30. M.J. Haun, E. Furman, S.J. Jang, and L.E. Cross, *Ferroelectrics*, **99**, 45 (1989).